Glasgow Caledonian University

University for the Common Good

Online monitoring and diagnosis of HV cable faults by sheath system currents

Dong, Xiang ; Yang, Yang; Zhou, Chengke; Hepburn, Donald M.

Published in:
IEEE Transactions on Power Delivery

DOI:
10.1109/TPWRD.2017.2665818

Publication date:
2017

Document Version
Author accepted manuscript

Link to publication in ResearchOnline

Citation for published version (Harvard):
Dong, X, Yang, Y, Zhou, C & Hepburn, DM 2017, 'Online monitoring and diagnosis of HV cable faults by sheath system currents', *IEEE Transactions on Power Delivery*, vol. 32, no. 5, pp. 2281-2290. https://doi.org/10.1109/TPWRD.2017.2665818

General rights
Copyright and moral rights for the publications made accessible in the public portal are retained by the authors and/or other copyright owners and it is a condition of accessing publications that users recognise and abide by the legal requirements associated with these rights.

Take down policy
If you believe that this document breaches copyright please view our takedown policy at https://edshare.gcu.ac.uk/id/eprint/5179 for details of how to contact us.

Download date: 04. May. 2023

On-line Monitoring and Diagnosis of HV Cable Faults by Metal Sheath System Currents

Xiang Dong, Yang Yang, *Student Member, IEEE*, Chengke Zhou, *Senior Member, IEEE*, and Donald M. Hepburn, *Member, IEEE*

***Abstract*— Cross-bonded metal sheath connection is applied in sectioned single-core power cables to reduce or eliminate the voltages which are induced in the sheath over long distances. However, cross-bonded cables present an opportunity as well as a challenge for on-line measurement and diagnosis of cable conditions. In this paper, a methodology to identify cable faults through analysis of the sheath system currents in a cross-bonded cable system is presented. Firstly, a numerical model is established to simulate the sheath currents in cross-bonded cable systems. Secondly, analyses of several faults, which happen frequently with serious consequences, are presented on the basis of current measurement at the link cable. Simulations of normal and fault conditions are given to determine the feasibility of fault diagnosis. A case study using field data from a cable tunnel in China considering the normal condition is presented to verify the numerical model. Results in normal condition show good consistency with field data with error less than 5%. Simulation results of fault conditions show that analysis of readings from 6 current sensors can distinguish different fault types and fault positions using the method proposed. Based on the analyses, criteria are established for sheath loop fault type diagnosis.**

***Index Terms*—Cross-bonded, on-line monitoring, metal sheath currents, fault diagnosis**

I. Introduction

High voltage (HV) cables are applied in urban transmission and distribution networks to meet the requirements of long distance and large capacity energy transmission [1]. As the length of the cable increases, there will be an increase in induced voltage in the metal sheath [2]. An excessive induced voltage may lead to breakdown in the outer sheath, and even failure of the insulation [3]. In addition, there will be circulating current in the metal sheath loop, which will limit the current rating of the power cables [4]. Consequently, cross-bonding of metal sheath connection at cable joints has been proposed to solve these problems [2].

However, during the service life, HV cables are also vulnerable to failures due to causes which could be classified into six groups, namely adverse environmental conditions, third party damage, poor workmanship, manufacturing problems, operational or maintenance reasons, and age related degradation [5].

According to statistics covering the last 20 years, the weakest points in cable systems were interfaces or junctions [4]. Under cross-bonding of the metal sheaths, the weakest interfaces at the major sections were joints, link boxes and terminals [3]. Cable metal sheath systems contain not only cable metal sheaths, but also the accessories for metal sheath connections, including joints, link boxes and terminals. It should be addressed that "sheath" hereafter specially refers to metal sheath in the paper. Among all the cable failure causes in cross-bonded cable systems, a good number of them are sheath system faults, such as flooded cable joints, corrosion or third party damage to the cable jackets and breakdown of insulating flanges in joint, result in excessive sheath currents. Open circuit faults in sheaths, due to the theft of earthing strips, has happened in the past.

The key to improving the identification, characterization and determination of the insulation condition is condition monitoring (CM) [6]. Many successes in identifying and localizing defects or faults through CM techniques have been reported: these include the monitoring of partial discharge (PD), insulation resistance (IR) and dielectric loss (DL) [7]. However, little work on on-line monitoring of cross-bonded cable systems based on sheath current has yet been reported.

Some researchers have investigated numerical models to calculate the sheath currents in cross-bonded cable systems in normal conditions, e.g. [15]. The model established in [8] presented the sheath currents generated by induced voltage. Marzinotto and Mazzanti in [9] presented the feasibility of cable sheath fault detection by metal sheath-to-ground currents at the ends of cross-bonded sections. Sheath currents contain the currents produced by both load currents and inductive currents itself with the leakage currents through insulation. When the lengths of cables in the three minor sections are the same, and the installation method is three-phase center-symmetric, due to the balance among the three phases, circulating currents can be ignored. However, in practical situations, the lengths of minor sections will be different, and the installation layout could be flat, resulting in unbalanced currents. As a result, sheath currents would be several Amperes and even tens of Amperes, which would limit the current rating of the cables.

This paper proposes the use of sheath system currents as indicators to detect cable sheath faults. It firstly presents a cross-bonded three phase cable model to determine metal

Xiang Dong is with China State Grid, Beijing Electric Power Company, (dongxiang0820@sina.com)

Yang Yang is with Glasgow Caledonian University, Glasgow, UK, G4 0BA (Yang.Yang@gcu.ac.uk)

Chengke Zhou is with Glasgow Caledonian University, Glasgow, UK, G4 0BA (c.zhou@gcu.ac.uk)

Donald M. Hepburn is with Glasgow Caledonian University, Glasgow, UK, G4 0BA (D.M.Hepburn@gcu.ac.uk)

sheath currents in normal operating conditions. Through theoretical analysis and simulation in MATLAB, the cable model is studied under normal conditions. On the basis of the work proposed in this paper, on-line measurements were carried out in a major section of a cross-bonded system in a cable tunnel in China. The field data was collected from the current sensors installed at link cables and the model results are verified by the field data. Then, three selected fault conditions are analyzed on the basis of expected values and the criteria for metal sheath fault diagnosis are given.

II. The Establishment of Model

A typical cross-bonded major cable section is illustrated in Fig. 1. There are 3 minor sections in each of the three phases. At both ends of the major section, the terminals or joints are connected to other cable sections, overhead lines or substation equipment. The metal sheaths at both ends of a major section are connected to the grounding boxes, G1 and G2, with direct grounding. Within a major section, the cable joints, JA1, JB1, JC1, JA2, JB2 and JC2, are constructed to connect different minor sections. The co-axial link cables connect the metal sheaths to the link boxes and the cross-bonded connections are implemented inside the link boxes, J1 and J2.

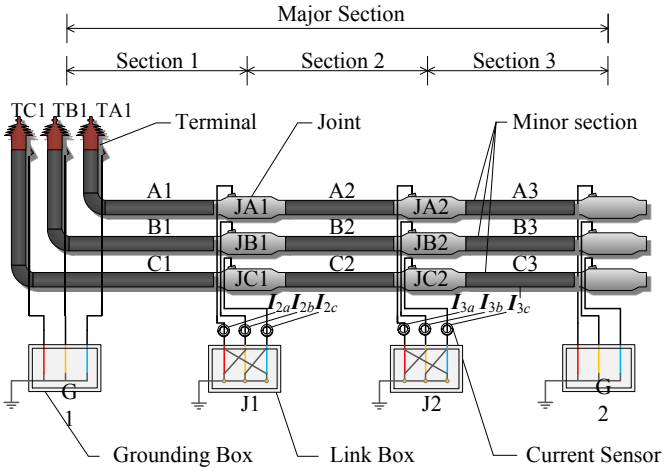

Fig. 1. A typical cross-bonded cable, showing major and minor sections

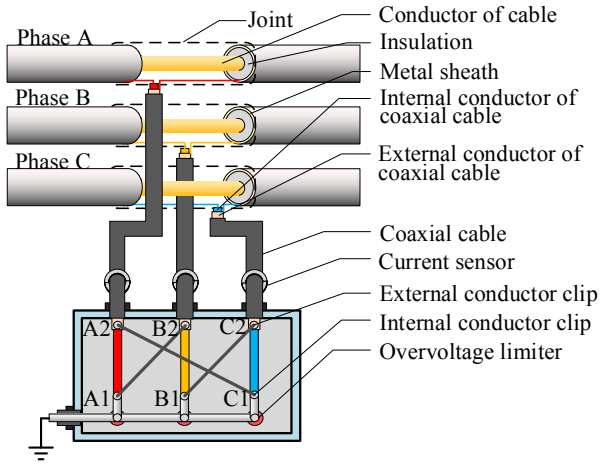

Fig. 2. A typical link box with co-axial cables connection [16]

Fig. 2 shows a typical link box with co-axial cable connections. In many parts of China, co-axial cables are used to bring the metal sheath conductors to the link boxes for ease of installation. Considering link box J1 from Fig.1, as indicated in Fig. 2, the sheath of A1 is connected to that of B2; B1 is connected to C2; C1 is connected to A2. Similarly, in link box J2 the connections would be: A2 connects to B3; B2 connects to C3; C2 connects to A3. However, the conductor clips in link box are open-circuited from the ground in normal condition due to the overvoltage limiter (OVL), when the voltages across the OVLs did not exceed 50 V. So the cross bonding among three phase sections would be A1-B2-C3 (loop 1), B1-C2-A3 (loop 2) and C1-A2-B3 (loop 3). Sheath current in each metal sheath loop composes of leakage current through the insulation and circulating current due to the unbalanced induced voltage in metal sheath loop, as shown in Fig. 3.

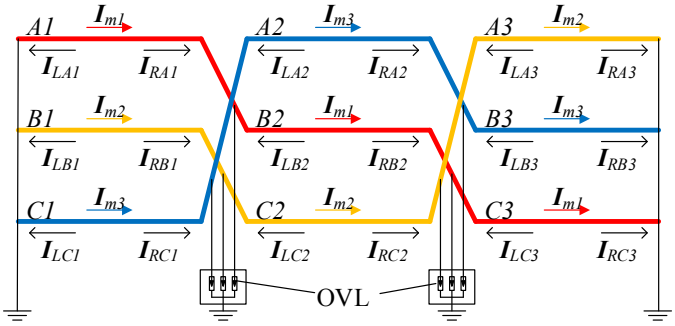

Fig. 3. The simplified cross bonded sheath connections with circulating currents and leakage currents [18]

Where, I_{mn} (n=1, 2, 3) is the circulating current in each sheath loop. *Xn* (X is A, B or C) is the minor section cable in different phase. I_{LXn} and I_{RXn} are the leakage current components in the left and right directions.

Fig.3 presents the simplified cross bonded sheath connections derived from Fig. 1 and Fig.2 for the understanding of leakage currents and circulating currents.

A. Leakage current

Leakage current is the current flowing through cable main insulation. And leakage current of each minor section can be calculated using Equation (1).

$$\boldsymbol{I}_l = \frac{\boldsymbol{U}}{\boldsymbol{Z}_i + \boldsymbol{Z}_e + \boldsymbol{Z}_S} \approx \frac{\boldsymbol{U}}{\boldsymbol{Z}_i} \tag{1}$$

Where, $\boldsymbol{Z}_i$ represents the insulation impedance of the cable section under consideration; $\boldsymbol{Z}_e$ is the equivalent impedance to the ground; $\boldsymbol{Z}_S$ is the equivalent impedance of the semi-conductive screen; $\boldsymbol{U}$ stands for the working voltage the cable is subjected to under normal operating conditions. It should be addressed that the symbols in bold indicate for vectors that contain phase and amplitude in this paper.

TABLE 1
COMPARISON OF THE IMPEDANCE OF DIFFERENT LAYERS

Layers	Impedance (Ω·m)
Semi-conductive screen	0.01~ 10
XLPE insulation	$> 500 \times 10^6$
Metal sheath	0.05×10^{-3}

From Table 1 [14], insulation impedance is much bigger than semi-conductive screen and metal sheath, this model ignores the semi-conductor layer as it has little influence on the results.

In this paper, operation voltage is taken to be a constant vector; while the insulation condition is taken to be unchanged during measurements. Consequently, the value of leakage current is unchanged when operation voltage and insulation condition is decided.

Leakage currents contain capacitive and resistive components. As insulation resistance in HV cables could reach hundreds of Giga-Ohms per kilometer, the resistive component would be less than 1 mA, while the capacitive component could be several Amps/km. So, leakage current can be approximated as capacitive current using Equation (2).

$$\boldsymbol{I}_l \approx \boldsymbol{I}_C = j\omega C \cdot \boldsymbol{U} \tag{2}$$

Generally, insulation capacitance is derived from Equation (3).

$$C = \frac{\varepsilon \times 55.6 \times 10^{-12}}{\ln(\frac{D_C + 2\delta_i}{D_C})} \tag{3}$$

Where, in this instance, ε is relative permittivity; D_C is the diameter of the cable conductor; δ_i is the thickness of cable insualtion.

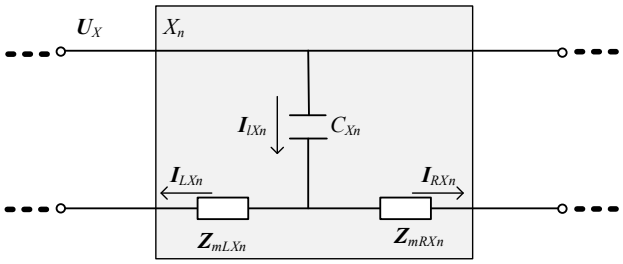

Fig. 4. The equivalent circuit of single phase cable (X_n) in a minor section

The simplified minor section is shown in Fig. 4. $\boldsymbol{U}_X$ (X stands for the symbol of a phase, i.e., A, B or C) is the voltage in core conductor. $\boldsymbol{I}_{lXn}$ (n=1, 2, 3) is the leakage current through the insulation in each minor section; C_{Xn} is the insulation capacitance in each minor section; Z_{mLXn} is the equivalent metal sheath impedance on the left side. While, Z_{mRXn} is the equivalent metal sheath impedance on the right side, when considering distribution of leakage current through insulation.

Sheath impedance of each minor section, Z_{mXn}, is the sum of Z_{mLXn} and Z_{mRXn}.

$$\boldsymbol{Z}_{mXn} = \boldsymbol{Z}_{mLXn} + \boldsymbol{Z}_{mRXn} \tag{4}$$

The leakage current components in Fig. 4, such as $\boldsymbol{I}_{LA1}$ and $\boldsymbol{I}_{RA1}$, are based on the distribution of the impedance in the sheaths. The leakage current components $\boldsymbol{I}_{LA1}$ and $\boldsymbol{I}_{RA1}$ can be obtained as:

$$\boldsymbol{I}_{LA1} = \frac{\boldsymbol{Z}_{mRA1} + \boldsymbol{Z}_{mB2} + \boldsymbol{Z}_{mC3} + R_g}{\boldsymbol{Z}_{mA1} + \boldsymbol{Z}_{mB2} + \boldsymbol{Z}_{mC3} + R_g + R_e} \cdot \boldsymbol{I}_{lA1} \tag{5}$$

$$\boldsymbol{I}_{RA1} = \frac{\boldsymbol{Z}_{mLA1} + R_e}{\boldsymbol{Z}_{mA1} + \boldsymbol{Z}_{mB2} + \boldsymbol{Z}_{mC3} + R_g + R_e} \cdot \boldsymbol{I}_{lA1} \tag{6}$$

B. Circulating current

As a HV cable system is always grounded at both ends of each major section for safety, it offers loops for circulating currents. When the vector sum of induced voltages, such as $\boldsymbol{u}_{SA1}$, $\boldsymbol{u}_{SB2}$ and $\boldsymbol{u}_{SC3}$ in metal sheath loop 1, are not zero due to the unbalanced section lengths and unbalanced installation type, there will be circulating current, $\boldsymbol{I}_{m1}$, as shown in Fig. 5.

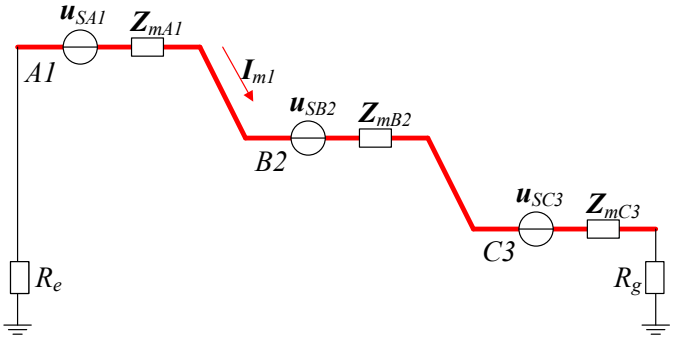

Fig. 5. The equivalent circuit of circulating current loop 1

In Fig. 3, the equations for the initial circulating currents are shown in Equations (7) - (9).

$$\boldsymbol{I}_{m1} = \frac{\boldsymbol{u}_{SA1} + \boldsymbol{u}_{SB2} + \boldsymbol{u}_{SC3}}{\boldsymbol{Z}_{mA1} + \boldsymbol{Z}_{mB2} + \boldsymbol{Z}_{mC3} + R_e + R_g} \tag{7}$$

$$\boldsymbol{I}_{m2} = \frac{\boldsymbol{u}_{SB1} + \boldsymbol{u}_{SC2} + \boldsymbol{u}_{SA3}}{\boldsymbol{Z}_{mB1} + \boldsymbol{Z}_{mC2} + \boldsymbol{Z}_{mA3} + R_e + R_g} \tag{8}$$

$$\boldsymbol{I}_{m3} = \frac{\boldsymbol{u}_{SC1} + \boldsymbol{u}_{SA2} + \boldsymbol{u}_{SB3}}{\boldsymbol{Z}_{mC1} + \boldsymbol{Z}_{mA2} + \boldsymbol{Z}_{mB3} + R_e + R_g} \tag{9}$$

Where, $\boldsymbol{u}_{SXn}$ (X stands for A, B or C; n=1, 2, 3) are the induced voltages in the sheath of each minor section; $\boldsymbol{Z}_{mXn}$ represents the equivalent sheath impedances; R_e and R_g are the earth resistances at the ends of the major cable section.

Circulating current flowing in the sheath mainly depends on the induced voltage in the metal sheath and the impedance of the metal sheath loop. Meanwhile, induced voltages are subject to the configuration of the major cable sections, load currents installation type and also circulating currents. As leakage current is much smaller than load current, its influence is ignored in the calculation of induced voltage.

The inductance coefficient of the conductor-to-metal sheath of each phase, L_S, is derived from Equation (10) [13].

$$L_S = 2 \cdot \ln(\frac{2}{D_S}) \cdot 10^{-7} \tag{10}$$

$$D_S = \frac{1}{2}(D_{Si} + D_{Se}) \tag{11}$$

Where, D_S is the average diameter of metal sheath. D_{Si} is internal diameter of the metal sheath. D_{Se} is external diameter of the metal sheath.

The phase-to-phase inductance coefficient of the sheath, M, is derived from Equation (12) [15].

$$M = 2 \cdot \ln(\frac{1}{S}) \cdot 10^{-7} \tag{12}$$

Where, S is the distance between phases.

Due to the thickness of the metal sheath is relatively small, the self-impedance of metal sheath is negligible.

Consequently, the induced voltages of metal sheath in minor sections are derived from Equations (13) - (21).

$$\boldsymbol{u}_{SA1} = -j\omega\cdot(\boldsymbol{I}_A\cdot L_S + (\boldsymbol{I}_B+\boldsymbol{I}_{m2})\cdot M_{AB} + (\boldsymbol{I}_C+\boldsymbol{I}_{m3})\cdot M_{AC})\cdot l_1 \quad (13)$$

$$\boldsymbol{u}_{SB1} = -j\omega\cdot(\boldsymbol{I}_B\cdot L_S + (\boldsymbol{I}_A+\boldsymbol{I}_{m1})\cdot M_{AB} + (\boldsymbol{I}_C+\boldsymbol{I}_{m3})\cdot M_{BC})\cdot l_1 \quad (14)$$

$$\boldsymbol{u}_{SC1} = -j\omega\cdot(\boldsymbol{I}_C\cdot L_S + (\boldsymbol{I}_A+\boldsymbol{I}_{m1})\cdot M_{AC} + (\boldsymbol{I}_B+\boldsymbol{I}_{m2})\cdot M_{BC})\cdot l_1 \quad (15)$$

$$\boldsymbol{u}_{SA2} = -j\omega\cdot(\boldsymbol{I}_A\cdot L_S + (\boldsymbol{I}_B+\boldsymbol{I}_{m1})\cdot M_{AB} + (\boldsymbol{I}_C+\boldsymbol{I}_{m2})\cdot M_{AC})\cdot l_2 \quad (16)$$

$$\boldsymbol{u}_{SB2} = -j\omega\cdot(\boldsymbol{I}_B\cdot L_S + (\boldsymbol{I}_A+\boldsymbol{I}_{m3})\cdot M_{AB} + (\boldsymbol{I}_C+\boldsymbol{I}_{m2})\cdot M_{BC})\cdot l_2 \quad (17)$$

$$\boldsymbol{u}_{SC2} = -j\omega\cdot(\boldsymbol{I}_C\cdot L_S + (\boldsymbol{I}_A+\boldsymbol{I}_{m3})\cdot M_{AC} + (\boldsymbol{I}_B+\boldsymbol{I}_{m1})\cdot M_{BC})\cdot l_2 \quad (18)$$

$$\boldsymbol{u}_{SA3} = -j\omega\cdot(\boldsymbol{I}_A\cdot L_S + (\boldsymbol{I}_B+\boldsymbol{I}_{m3})\cdot M_{AB} + (\boldsymbol{I}_C+\boldsymbol{I}_{m1})\cdot M_{AC})\cdot l_3 \quad (19)$$

$$\boldsymbol{u}_{SB3} = -j\omega\cdot(\boldsymbol{I}_A\cdot L_S + (\boldsymbol{I}_A+\boldsymbol{I}_{m2})\cdot M_{AB} + (\boldsymbol{I}_C+\boldsymbol{I}_{m1})\cdot M_{BC})\cdot l_3 \quad (20)$$

$$\boldsymbol{u}_{SC3} = -j\omega\cdot(\boldsymbol{I}_A\cdot L_S + (\boldsymbol{I}_A+\boldsymbol{I}_{m1})\cdot M_{AC} + (\boldsymbol{I}_B+\boldsymbol{I}_{m2})\cdot M_{BC})\cdot l_3 \quad (21)$$

Where, M_{AB} is the phase-to-phase inductance between phase A and B; M_{AC} is the phase-to-phase inductance between phase A and C; M_{BC} is the phase-to-phase inductance between phase B and C; l_1, l_2 and l_3 are the lengths of the three sections. The initial value of circulating current in each metal sheath loop is zero.

The unit resistance of the metal sheath, R_m, can be expressed by Equation (22) [17].

$$R_m = \frac{k_r(1+k_t(T-20))}{\pi((\frac{D_{Se}}{2})^2-(\frac{D_{Si}}{2})^2)} \quad (22)$$

In this example, k_r is the metal sheath resistivity; k_t is metal sheath temperature coefficient; T is ambient temperature.

The unit impedance of the three metal sheath loops, from loop 1 to loop 3, are expressed by Equations (23).

$$\boldsymbol{Z}_m = R_m + jX_m \quad (23)$$

$$X_m = 2\ln(2\times\sqrt[3]{2}S/D_S)\times10^{-7} \quad (24)$$

Where, Xm is the unit average inductance of sheath in minor section [17].

From the above, the iterative procedure for solving the circulating current is shown in Fig. 6.

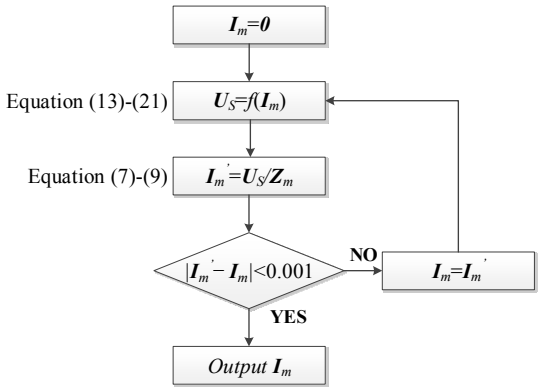

Fig. 6. The iteration steps for calculating circulating current [16][19]

C. Detected current

The resultant metal sheath current in each of the three metal sheath paths is the sum of the leakage currents as determined from Equations (1) - (6) and the circulating currents from iterative procedures.

Owing to the application of co-axial cables to connect joints and link boxes, a current sensor installed on a co-axial cable leading to a cable link box will detect the vector sum of two different metal sheath currents. Based on the installation of current sensors shown in Fig. 1 and Fig. 2, the detected currents by current sensors are shown in Fig.7 and given by Equations (25) - (30):

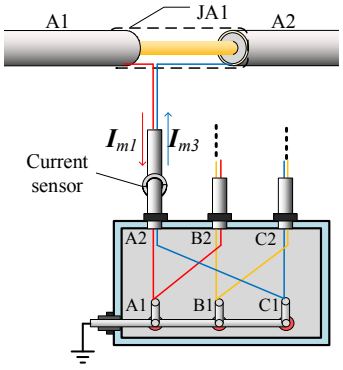

Fig. 7. The detected current by the current sensor I_{2a} (modified from fig. 2)

$$\boldsymbol{I}_{2a} = (\boldsymbol{I}_{m1}+\boldsymbol{I}_{RA1}-\boldsymbol{I}_{LB2}-\boldsymbol{I}_{LC3})-(\boldsymbol{I}_{m3}+\boldsymbol{I}_{RC1}-\boldsymbol{I}_{LA2}-\boldsymbol{I}_{LB3}) \quad (25)$$

$$\boldsymbol{I}_{2b} = (\boldsymbol{I}_{m2}+\boldsymbol{I}_{RB1}-\boldsymbol{I}_{LC2}-\boldsymbol{I}_{LA3})-(\boldsymbol{I}_{m1}+\boldsymbol{I}_{RA1}-\boldsymbol{I}_{LB2}-\boldsymbol{I}_{LC3}) \quad (26)$$

$$\boldsymbol{I}_{2c} = (\boldsymbol{I}_{m3}+\boldsymbol{I}_{RC1}-\boldsymbol{I}_{LA2}-\boldsymbol{I}_{LB3})-(\boldsymbol{I}_{m2}+\boldsymbol{I}_{RB1}-\boldsymbol{I}_{LC2}-\boldsymbol{I}_{LA3}) \quad (27)$$

$$\boldsymbol{I}_{3a} = (\boldsymbol{I}_{m3}+\boldsymbol{I}_{RC1}+\boldsymbol{I}_{RA2}-\boldsymbol{I}_{LB3})-(\boldsymbol{I}_{m2}+\boldsymbol{I}_{RB1}+\boldsymbol{I}_{RC2}-\boldsymbol{I}_{LA3}) \quad (28)$$

$$\boldsymbol{I}_{3b} = (\boldsymbol{I}_{m1}+\boldsymbol{I}_{RA1}+\boldsymbol{I}_{RB2}-\boldsymbol{I}_{LC3})-(\boldsymbol{I}_{m3}+\boldsymbol{I}_{RC1}+\boldsymbol{I}_{RA2}-\boldsymbol{I}_{LB3}) \quad (29)$$

$$\boldsymbol{I}_{3c} = (\boldsymbol{I}_{m2}+\boldsymbol{I}_{RB1}+\boldsymbol{I}_{RC2}-\boldsymbol{I}_{LA3})-(\boldsymbol{I}_{m1}+\boldsymbol{I}_{RA1}+\boldsymbol{I}_{RB2}-\boldsymbol{I}_{LC3}) \quad (30)$$

Where, $\boldsymbol{I}_{nx}$ (n= 2 or 3. x represents a, b or c) is detected currents from current sensors installed at co-axial cables. $\boldsymbol{I}_{mn}$ (n = 1, 2 or 3) is circulating current. $\boldsymbol{I}_{LXn}$ and $\boldsymbol{I}_{RXn}$ are leakage current components in left and right directions in Xn minor section.

Overall, as sheaths are grounded at both end of a major section, there will be leakage currents in metal sheath loops. Moreover, flat type installation and unbalanced length among three sections will lead to circulating currents in metal sheath loops. Furthermore, current sensors installed at co-axial link cables will detect the vector sum of two different metal sheath currents. The detected currents will be applied to localize the sheath faults in Section III.

III. Verification of Model in Normal Condition

The on-line monitoring methodology outlined above was applied to a major section under 110 kV shown in Fig. 8. The parameters of the major section are listed in Table 2. The installation of the current sensors is based on Fig. 1 and Fig. 2. The 6 current sensors in this major section are respectively labelled $\boldsymbol{I}_{2a}$, $\boldsymbol{I}_{2b}$, $\boldsymbol{I}_{2c}$, $\boldsymbol{I}_{3a}$, $\boldsymbol{I}_{3b}$ and $\boldsymbol{I}_{3c}$ for later use.

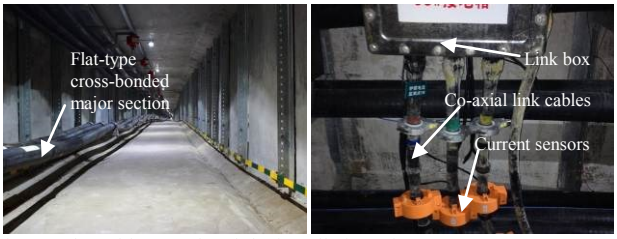

Fig. 8. The cable tunnel and the installation of current sensors

TABLE 2
DATA OF THE EXAMPLE CABLE CIRCUIT

Parameters	Value
Diameter of all the three cable conductors (m)	38.9×10^{-3}
Thickness of cable insulation (m)	16×10^{-3}
Relative permittivity of insulation	2.3
External diameter of the metal sheath (m)	99.6×10^{-3}
Internal diameter of the metal sheath (m)	97.3×10^{-3}
Metal sheath temperature coefficient (10^{-6}/°C)	4.03×10^{-3}
Metal sheath resistivity (Ω·m)	2.84×10^{-8}
Distance between phase A and B (m)	0.27
Distance between phase B and C (m)	0.27
Distance between phase A and C (m)	0.54
Ambient temperature (°C)	35
Phase-to-phase operation voltage (kV)	110
Grounding resistance at sub-station side (Ω)	0.2
Length of section 1 (m)	425
Length of section 2 (m)	477
Length of section 3 (m)	536

The load currents of the three phases on 2016-01-04 are shown in Fig. 9, where the data presented is the RMS values of load currents collected every 6 minutes, altogether 240 samples. The sampling time of 2 seconds means that each value contains 100 cycles.

The measured load currents, as shown in Fig. 8, are applied to the model to calculate the currents which would be expected in the current sensors. The results of the calculations and the field data are shown in Fig.10 and Fig. 11 respectively.

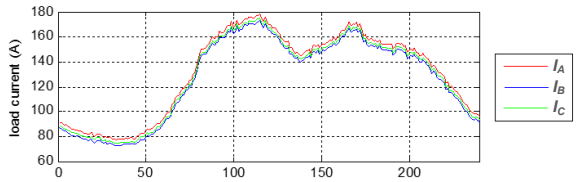

Fig. 8. RMS values of load currents of three phases on 2016-01-04

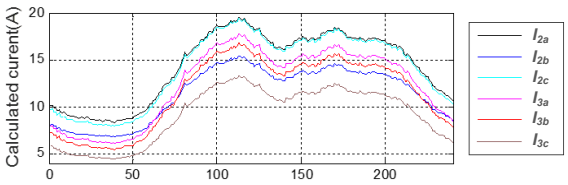

Fig. 9. Calculated currents based on load currents measured on 2016-01-04

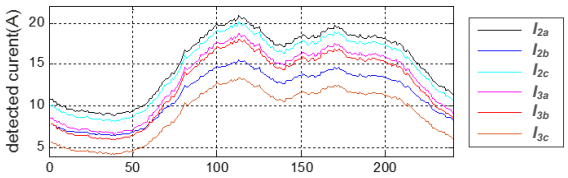

Fig. 10. Detected currents from the current sensors on 2016-01-04

TABLE 3
COMPARISON BETWEEN CALCULATED AND DETECTED CURRENTS AT 2016-01-04T11:48 (MAX ERROR TIME POINT)

	I_{2a}	I_{2b}	I_{2c}	I_{3a}	I_{3b}	I_{3c}
Calculated current (A)	20.61	15.42	20.02	18.05	17.42	13.03
Detected current (A)	19.58	15.3	19.57	17.53	16.61	13.02
Error (%)	4.997	0.778	2.248	2.881	4.650	0.076

There are subtle differences between the information in Fig. 10 and Fig. 11. To make the difference between expected and detected currents clear, the results at a given sampling time, namely 2016-01-04T11:48 (11.48 am on the 4th of January 2016), are shown in Table 3. The error between simulated currents and field data is less than 5%. And the validation has also been done from 2015-05 to 2016-01. The results showed good consistency with error less than 5%.

In Table 3, the six currents, $\boldsymbol{I}_{2a}$, $\boldsymbol{I}_{2b}$, $\boldsymbol{I}_{2c}$, $\boldsymbol{I}_{3a}$, $\boldsymbol{I}_{3b}$ and $\boldsymbol{I}_{3c}$ are the current detected by current sensors installed as shown in Fig.1. Although, ideally, the metal sheath current should be exactly offset by cross-bonded connection, the detected currents have non-zero values. There are several reasons for this under normal operating conditions, namely:

1) The flat cable installation method leads to imbalanced voltages in the metal sheaths, as indicated in Equation (7) - (9).
2) When the metal sheaths are grounded at both ends of the major section, the leakage current components in metal sheath current could reach several Amps/km in HV cables.
3) Most importantly, as the lengths of the three minor sections of the major cross-bonded section are imbalanced, different induced voltages result.

It should be noted that the errors between calculated and measured currents are less than 5% during the measuring period. This could meet the requirement of on-line monitoring of metal sheath current in HV cross-bonded major section.

IV. DETECTION AND ANALYSIS OF ABNORMAL CONDITIONS

This section considers 12 fault conditions, those which are the most likely to occur in a cross-bonded cable system, as presented in Table 4. These faults belong to 3 types, i.e. open circuit of the metal sheath loops, flooded cable link box and insulation breakdown between metal sheath conductors.

The case studies analyzed in the calculations are undertaken in a major section of 110 kV with equal lengths of 500 m in each minor section, which is a typical case in cross bonded connections.

TABLE 4
SIMULATED FAULT CONDITIONS

	Fault point
1	Open-circuit fault in metal sheath loop1 (A1-C2-B3)
2	Open-circuit fault in metal sheath loop2 (B1-A2-C3)
3	Open-circuit fault in metal sheath loop3 (C1-B2-A3)
4	Short-circuit fault due to flooding in link box J1
5	Short-circuit fault due to flooding in link box J2
6	Short-circuit fault due to flooding in link boxes J1 and J2
7	Insulation breakdown in joint JA1
8	Insulation breakdown in joint JB1
9	Insulation breakdown in joint JC1
10	Insulation breakdown in joint JA2
11	Insulation breakdown in joint JB2
12	Insulation breakdown in joint JC2

A. Open-circuit fault in one metal sheath loop

Disconnection of a metal sheath loop is a common fault in cross-bonded cable systems [10]. This may be the result of loose connections due to corrosion, poor installation practice

or third party damage. To address this, the work focuses on metal sheath fault diagnosis of disconnections in terminals and joints and the impact of this fault type are examined. A disconnection of sheath in terminal TA1 is used as an example.

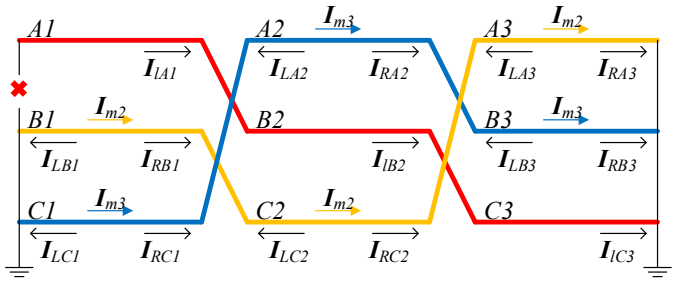

Fig. 12. Equivalent circuit of open-circuit in the metal sheath in terminal

Fig. 12 assumes that loop 1 is disconnected as an open circuit point in terminal TA1. As a result, there will be no circulating current in metal sheath loop 1, and leakage currents of A1, B2 and C3 section will flow into the ground at the right. The current sensors I_{2a}, I_{2b}, I_{3b} and I_{3c} would be affected as they detect the metal sheath current of loop 1, while I_{2c} and I_{3a} will only detect the metal sheath currents of loop 2 and loop 3.

As the structure of loop 1 is changed, leakage currents in this metal sheath loop will redistribute. After analyzing the effects of the disconnections in loops at different terminals or joints, the current level results shown in Fig. 13 are generated.

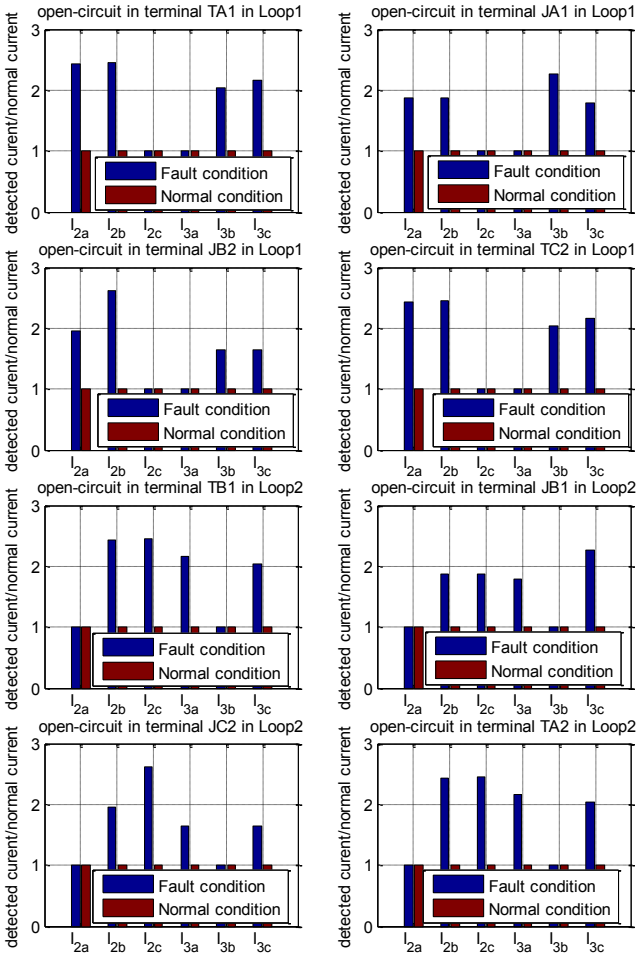

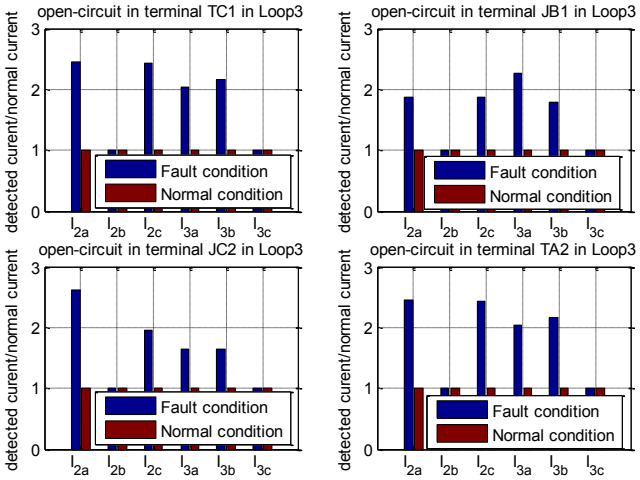

Fig. 13. The results of open-circuit faults in terminals and joints

It can be seen that for a fault in loop 1, although the values of I_{2c} and I_{3a} are unchanged by the fault conditions, the magnitude of variation in the other four sensors could provide indication of the fault location. Similarly, for a fault in loop 2, values from I_{2a} and I_{3b} are unchanged, and for a fault in loop 3, values of I_{2b} and I_{3c} are unchanged. Consequently, the faults could be divided into 3 groups. The criteria for open-circuit fault localization are expressed in Table 5.

TABLE 5
THE CRITERIA FOR DETECTION OF OPEN-CIRCUIT FAULTS BASED ON THE DETECTED CURRENTS

Open-circuit loop	Fault type determination	Judgment based on detected currents
Loop1 (A1-B2-C3)	$\mathrm{Max}(I_f)/I_n<3$	$(I_{2a}, I_{2b}, I_{2c}, I_{3a}, I_{3b}, I_{3c})$ = (1,1,0,0,1,1)
Loop2 (B1-C2-A3)	$\mathrm{Max}(I_f)/I_n<3$	$(I_{2a}, I_{2b}, I_{2c}, I_{3a}, I_{3b}, I_{3c})$ = (0,1,1,1,0,1)
Loop3 (C1-A2-B3)	$\mathrm{Max}(I_f)/I_n<3$	$(I_{2a}, I_{2b}, I_{2c}, I_{3a}, I_{3b}, I_{3c})$ = (1,0,1,1,1,0)

In Table 5, "1" means obvious variation (difference between detected current and that in normal condition is much more than 5 % which is the maximum difference under normal conditions with no fault) in detected current and "0" means no obvious variation in detected current; I_f is the detected current in fault condition; I_n is the detected current in normal condition.

In case of an open-circuit fault in a sheath loop, some detected currents are not much different from that in normal condition due to there is no fault in that detected sheath loops. Meanwhile, the fault current is relatively low in comparison with load current leading to little effect on the sheath associated with the phases without fault. So this characteristic could be used for the detection of open-circuit fault in sheath loops.

B. Flooded cable link box

In sub-tropical areas, HV cables installed in cable tunnels may be immersed in water for several months in each calendar year. When a cable link box is damaged, the conductors in the box would be immersed in water. Under certain circumstances the resistance of the water is low and the protective earthing inside the link box will be bypassed, resulting in an alteration

to the paths of metal sheath current.

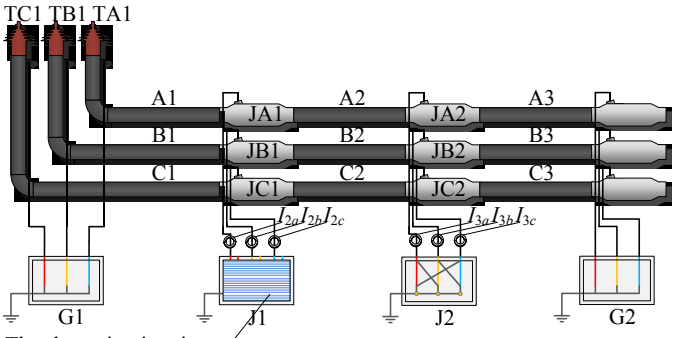

Fig. 14. Short-circuit fault due to ~~a~~ flooding in link box J1

Taking flooding of link box J1 as a fault example, Fig. 14 presents a short-circuit fault due to a flood in link box J1. The metal sheath of sections A1, A2, B1, B2, C1 and C2 will be grounded at link box J1 and the resulting circulating currents will change. There are 6 loops, which are A1, B1, C1, A2-B3, B2-C3 and C2-A3 loops, as shown in Fig 15. In each loop, the circulating current is based on the induced voltage in the metal sheath, while leakage current in each section will redistributed. In each new loop, the induced voltage will not be offset. As a result, there will be relatively high circulating current in each new loop in comparison with normal condition.

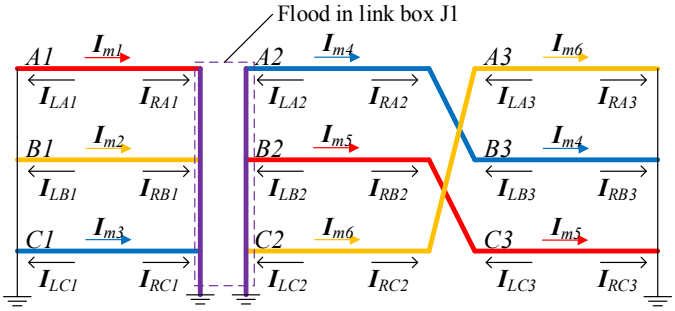

Fig. 15. Equivalent circuit of short-circuit fault due to ~~a~~ flooding in link box J1

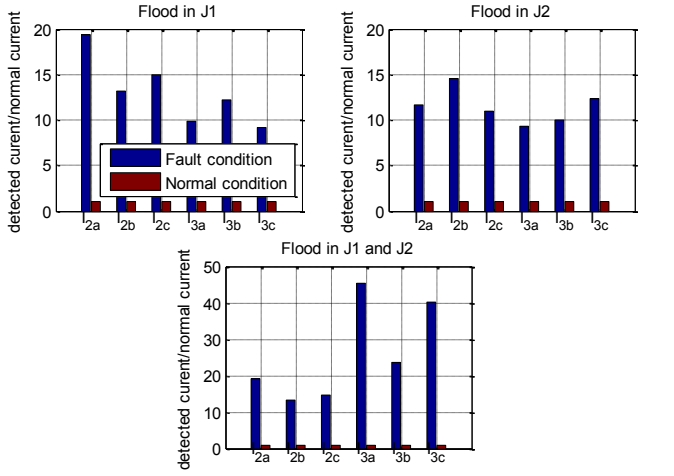

Fig. 16. Results of the flooding faults in link boxes in different conditions

In the first graph of Fig. 16, it is the simulated output of each current sensor resulting from a flood fault in link box J1. The detected current in $\boldsymbol{I}_{2a}$, will reach almost 40 A, while the detected currents in $\boldsymbol{I}_{2b}$, and $\boldsymbol{I}_{2c}$, are about 30 A. This kind of fault, which may affect the ampacity and even lead to more serious failure, should be diagnosed immediately. As shown in Fig. 16, flooding in different link boxes will lead to an obvious increase in detected currents in comparison with those in the normal conditions. As a result, the detected currents can be used to identify the metal sheath loop circuit faults.

A flood in a grounding box still results the same as grounding directly, the same function as grounding box. So this fault condition is not discussed in the paper. Table 6 indicates the criteria for fault identification.

TABLE 6
THE CRITERIA FOR DETECTION OF FLOOD FAULTS BASED ON THE DETECTED CURRENTS

Short-circuit due to flood in link box	Fault type determination	Judgment based on detected currents
Flood in link box J1	Min(I_f)/I_n>5	(I_{2a}, I_{2b}, I_{2c}) = (1,0,0) (I_{3a}, I_{3b}, I_{3c}) = (0,1,0)
Flood in link box J2	Min(I_f)/I_n>5	(I_{2a}, I_{2b}, I_{2c}) = (0,1,0) (I_{3a}, I_{3b}, I_{3c}) = (0,0,1)
Flood in link boxes J1 and J2	Min(I_f)/I_n>5	(I_{2a}, I_{2b}, I_{2c}) = (1,0,0) (I_{3a}, I_{3b}, I_{3c}) = (1,0,0)

In regard to Table 6, "1": highest among three detected currents. "0": relative lower among three detected currents (Max (I_f)-I_f^*) $\geqslant$ 10 A).

In simulation, the value of fault impedance, R_f, used in simulation is assumed as ranging from 0 to 1 Ω, as the water impedance is negligible. Although the current magnitudes varied, the results are not affected by fault impedance values, i.e. the criteria are still appropriate. As the variations of the detected currents are large in comparison with that in normal condition, these criteria are very effective for identifying the fault types and fault locations.

C. Breakdown of insulation between cable metal sheaths

When insulating flange between metal sheaths at both sides of a cable joint fails, there will be a short circuit between the failed metal sheaths, as shown below.

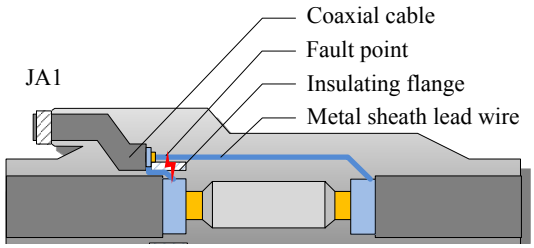

Fig. 17 (a). Short-circuit fault in insulating flange

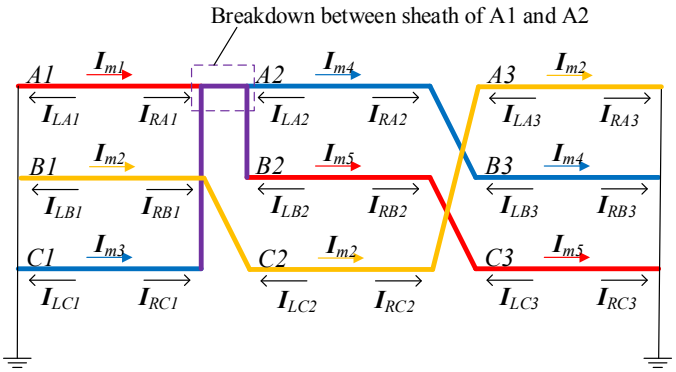

Fig. 17(b). Equivalent circuit of short-circuit fault due to the breakdown point between A1 and A2 metal sheath in joint JA1

Fig. 17 indicates a short contact between the metal sheaths of A1 and A2 in joint JA1. There will be a short connection between metal sheath loop 1 and 2. As the induced voltages in the metal sheaths will not be offset, there will be unbalanced currents in metal sheath loops. Sheath loop 2 will be influence little in this fault condition.

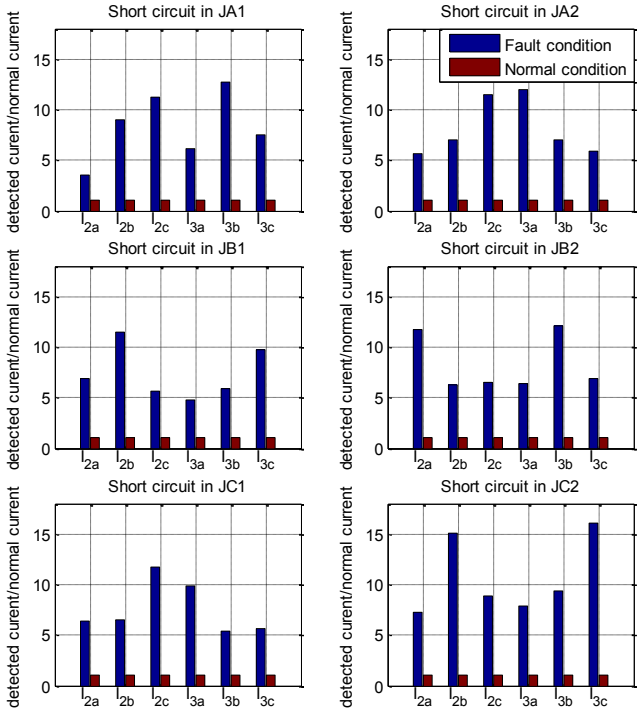

Fig. 18. Results of a short-circuit fault due to a breakdown between the sheath in joints

The results of multiple simulations of a range of fault positions are presented in Fig.18. Taking the short-circuit fault in JA1 as an example, fault currents are much higher than in normal conditions, as the two different sheath loops are short-connected. The induced voltage in each minor section could not be offset. Meanwhile, there is phase differences between the sheath currents in each minor section, so the fault currents in sheaths will superimposed. The results for different fault position present visible difference, which allows the localization of fault type and fault position. The criteria for identifying faults are given in Table 7.

TABLE 7
THE CRITERIA FOR DETECTION OF SHORT-CIRCUIT FAULTS DUE TO BREAKDOWN IN JOINTS BASED ON THE DETECTED CURRENTS

Short-circuit due to breakdown in joints	Fault type determination	Judgment based on detected currents
Breakdown in JA1	Max(I_f)/I_n >10	(I_{2a}, I_{2b}, I_{2c}, I_{3a}, I_{3b}, I_{3c}) =(1, 2, 3, 2, 3, 2)
Breakdown in JB1	Max(I_f)/I_n >10	(I_{2a}, I_{2b}, I_{2c}, I_{3a}, I_{3b}, I_{3c}) =(2, 3, 2, 1, 2, 2)
Breakdown in JC1	Max(I_f)/I_n >10	(I_{2a}, I_{2b}, I_{2c}, I_{3a}, I_{3b}, I_{3c}) =(2, 2, 3, 2, 1, 1)
Breakdown in JA2	Max(I_f)/I_n >10	(I_{2a}, I_{2b}, I_{2c}, I_{3a}, I_{3b}, I_{3c}) =(2, 2, 3, 3, 2, 2)
Breakdown in JB2	Max(I_f)/I_n >10	(I_{2a}, I_{2b}, I_{2c}, I_{3a}, I_{3b}, I_{3c}) =(3, 2, 2, 2, 3, 2)
Breakdown in JC2	Max(I_f)/I_n >10	(I_{2a}, I_{2b}, I_{2c}, I_{3a}, I_{3b}, I_{3c}) =(2, 3, 2, 2, 2,3)

In regard to Table 7, "3": $I_f^*/I_n > 10$. "2": Relative higher among three detected currents ($10 \geq I_f^*/I_n > 5$). "1": Relative change in comparison with that in normal condition ($I_f^*/I_n \leq 5$).

When the insulating flange suffers a breakdown, a short circuit happens between different sheath loops. So short connection happens between different sheath loops leading to increase of sheath currents. Usually, two of the detected currents are much higher than the other four detected currents. And the highest detected current would not exceed 20 times in comparison with that in normal condition.

V. CONCLUSION AND DISCUSSION

This paper presented a numerical model for cross-bonded HV cables, a methodology for simulation of metal sheath currents and the use of the model for determining the metal sheath currents under normal condition and three selected sets of fault conditions in a 1.5 km HV cross-bonded major section of equal length.

In the simulation, three kinds of metal sheath faults have been studied, namely open-circuit faults in metal sheath loop, short-circuit faults due to flood in link boxes and short-circuit faults due to breakdown between metal sheaths in joints. The faults investigated in this paper can be identified separately and localized to a particular metal sheath loop using the criteria proposed. As the criteria are based on comparison of the relative current magnitudes, the proposed method is robust as it is not affected by the impedance values in the metal sheath path.

The validity of the model is verified by use of field data collected from a set of cables in a cable tunnel, which is the cross-bonded connection. Comparison of simulated currents with measured values shows good consistency, i.e. error is less than 5% during a day of monitoring.

1) In normal conditions, due to the unbalanced length, load current and space layout of the cross-bonded major section, induced voltages may not be offset completely. Therefore, several and even tens of amperes circulating current is possible. So long length cross-bonded cable installation should be symmetrical to avoid circulating current.
2) In case of an open-circuit fault in a sheath loop, some detected currents not much different from that in

normal conditions due to there is no fault in some sheath loops. Meanwhile, the fault current is relatively low in comparison with load current leading to little effect on the sheath associated with the phases without fault. So this characteristic could be used for the detection of open-circuit fault in sheath loop.

3) In case of a short-circuit fault due to flooding in link box, due to the multi-grounding of sheath loop, induced voltage in each metal sheath lead to high circulating current between each grounding point. All detected currents will increase to more than 5 times in comparison with normal condition.
4) When the insulating flange at a cable joint suffers a breakdown, a short circuit happens between different sheath loops. Short connection then happens between different sheath loops leading to increasing of sheath currents. Usually, two of the detected currents are much higher than the other four detected currents. And the highest detected current would not exceed 20 times in comparison with that in normal condition.

In summary, the proposed cable diagnosis based on on-line monitoring of metal sheath currents in cross-bonded major section could be applied to help the metal sheath fault detection and localization in HV cable systems with cross-bonded connection. Laboratory experiments will be carried out to verify the model in fault conditions in future works.

VI. References

[1] J. Song-Manguelle, M. Harfman Todorovic, S. Chi, S. Gunturi and R. Datta, "Power Transfer Capability of HVAC Cables for Subsea Transmission and Distribution Systems", *IEEE Transactions on Industry Applications,* vol. 50, no. 4, pp. 2382-2391, 2014.

[2] M. D'Amore, M. Sarto and A. Scarlatti, "Modeling of magnetic-field coupling with cable bundle harnesses", *IEEE Transactions on Electromagnetic Compatibility*, vol. 45, no. 3, pp. 520-530, 2003.

[3] "IEEE Draft Guide for Bonding Metal sheaths and Shields of Single-Conductor Power Cables Rated 5 - 500 kV". *IEEE*, pp.1 -80.

[4] "IEEE Standard for the Testing, Design, Installation, and Maintenance of Electrical Resistance Trace Heating for Industrial Applications - Redline", *IEEE*, pp. 1-143, 2011.

[5] Z. Tang, C. Zhou, W. Jiang, W. Zhou, X. Jing, J. Yu, B. Alkali and B. Sheng, "Analysis of Significant Factors on Cable Failure Using the Cox Proportional Hazard Model", *IEEE Transactions on Power Delivery,* vol. 29, no. 2, pp. 951-957, 2014.

[6] Bojie Sheng, Wenjun Zhou, Jianhui Yu, Shaoxin Meng, Chengke Zhou and D. Hepburn, "On-line PD detection and localization in cross-bonded HV cable systems", *IEEE Transactions on Dielectrics and Electrical Insulation*, vol. 21, no. 5, pp. 2217-2224, 2014.

[7] R. Bartnikas, "Partial discharges. Their mechanism, detection and measurement", *IEEE Transactions on Dielectrics and Electrical Insulation*, vol. 9, no. 5, pp. 763-808, 2002.

[8] J. Barrett and G. Anders, "Circulating current and hysteresis losses in screens, metal sheaths and armour of electric power cables — mathematical models and comparison with IEC Standard 287", *IEE Proceedings - Science, Measurement and Technology,* vol. 144, no. 3, pp. 101-110, 1997.

[9] M. Marzinotto and G. Mazzanti, "The Feasibility of Cable Metal sheath Fault Detection by Monitoring Metal sheath-to-Ground Currents at the Ends of Cross-Bonding Sections", *IEEE Transactions on Industry Applications*, vol. 51, no. 6, pp. 5376-5384, 2015.

[10] A. Heaton and A. Issa, "Transient response of cross-bonded cable systems", *Proc. Inst. Electr. Eng. UK*, vol. 117, no. 3, p. 578, 1970.

[11] Y. Li, P. Fa-dong, C. Xiao-lin, C. Yong-hong and X. Li, "Study on Metal sheath Circulating Current of Cross-linked Power Cables", *2008 International Conference on High Voltage Engineering and Application*, 2008.

[12] Wang Wei., *XLPE insulated power cable technical basis*. Xi'an: *Northwestern Polytechnic University Press*, 1998.

[13] X. Dong, Y. Yuan, Z. Gao, C. Zhou, P. Wallace, B. Alkali, B. Sheng and H. Zhou, "Analysis of cable failure modes and cable joint failure detection via metal sheath circulating current", *2014 IEEE Electrical Insulation Conference (EIC)*, 2014.

[14] F. Guo, G. Zhu and X. Dong, "A method of 20 kV cable line fault location based on metal sheath grounding current", *2015 IEEE Industry Applications Society Annual Meeting*, 2015.

[15] C. Jung, J. Lee, J. Kang, X. Wang and Y. Song, "Metal sheath current characteristic and its reduction on underground power cable systems", *IEEE Power Engineering Society General Meeting, 2005*.

[16] Y. Yang, D. Hepburn, C. Zhou, W. Jiang, B. Yang and W. Zhou, "On-line monitoring and trending of dielectric loss in a cross-bonded HV cable system", *2015 IEEE 11th International Conference on the Properties and Applications of Dielectric Materials (ICPADM)*, 2015.

[17] G. Anders, Rating of electric power cables. New York: Institute of Electrical and Electronics Engineers, 1997.

[18] C. Jung, J. Lee, J. Kang, X. Wang and Y. Song, "Characteristics and Reduction of Sheath Circulating Currents in Underground Power Cable Systems", *International Journal of Emerging Electric Power Systems*, vol. 1, no. 1, 2004.

[19] Zhonglei Li, B. X. Du, L. Wang, C. Yang and H. J. Liu, "The calculation of circulating current for the single-core cables in Smart Grid," IEEE PES Innovative Smart Grid Technologies, Tianjin, 2012, pp. 1-4.

VII. Acknowledgment

The authors gratefully acknowledge the contributions of Wuhan Power Supply Company, China State Grid, who supplied field data and supported development of this paper.

VIII. Biographies

Xiang Dong was born in China. He received the B.Sc. degree from the North China Electrical Power University, China in 2011. He received the Ph.D. degree in Glasgow Caledonian University in 2014. Since then, he worked in China State Grid, Beijing Electric Power Company. His research interests are circulating and leakage current in cable metal sheath and condition monitoring of power cables.

Yang Yang was born in Hubei, China in 1991. He received the B.Sc. degree from Wuhan University of Technology in 2013. He received Master degree from Wuhan University in 2016. And now he is a Ph.D. student in Glasgow Caledonian University, who is mainly research on the development of the measurement of insulation condition, including dielectric loss, leakage current and insulation resistance.

Chengke Zhou (M'06, SM'13) received the B.Sc. and M.Sc. degrees in electrical engineering from HuaZhong University of Science and Technology, China in 1983 and 1986, respectively, and the Ph.D. degree at the University of Manchester U.K., in 1994. Since then, he worked in Glasgow Caledonian University (GCU), as a Lecturer and Senior Lecturer, and in Heriot-Watt University as a Reader. In 2007 he returned to GCU as a Professor. He has published more than 130 papers in the area of PD based condition monitoring of MV/HV plant and power system analysis. He is senior member of IEEE and Fellow of IET.

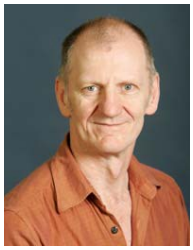

Donald M Hepburn (M'08) received his B.A. (Hons) from the Open University in 1987 and the Ph.D. degree from Glasgow Caledonian University (GCU) in 1994. He is a Senior Lecturer at GCU, a member of the IEEE, Institute of Physics, the IET and C.Eng.

He has 20 years of industrial research experience and has been involved in research into HV insulation systems at GCU for over 20 years. His research interests cover monitoring physical and chemical change in HV/MV insulation materials and application of advanced digital signal processing to information from electrical, acoustic and RF monitoring techniques.